Journal of Fluids and Structures (1999) **13,** 443–460
Article No.: jfls.1999.0213 available online at http://www.idealibrary.com on IDEAL

DYNAMICS OF A SUBMERGED AND INCLINED CONCENTRIC PIPE SYSTEM WITH INTERNAL AND EXTERNAL FLOWS

X. WANG† AND F. BLOOM‡

†*Institute of Paper Science and Technology, Atlanta, GA 30318, U.S.A.*
‡*Department of Mathematical Sciences, Northern Illinois University, DeKalb, IL 60115, U.S.A.*

(Received 19 January 1998 and in revised form 8 December 1998)

In this paper, we formulate a mathematical model to study the dynamics of submerged and inclined concentric pipes with different lengths. The governing equations of motion for the inner pipe are derived under small deformation assumptions and with the consideration of gravitational forces, turbulent boundary layer thickness of external flow, fluid frictional forces, and inertia effects. We obtain discretized dynamical equations using spatial finite-difference schemes and calculate the resonant frequencies of a particular pipe system design. In addition, by varying the operating conditions, we identify a few critical parameters pertaining to the proper design of such pipe systems.

1. INTRODUCTION

IN THE PAPER INDUSTRY, approach flow systems used to dilute fiber stock with water generally consist of many pumps, screens, deaerators, and piping components. One of the key components in these systems is the so-called silo water mixing unit, a cylindrical water storage tank with a constant water level, as depicted in Figure 1. The inner pipe protruding into the fan pump inlet zone contains a higher consistency fiber stock, and the concentric outer pipe collects the recirculation diluted stock. At the inlet end, the outer pipe is welded on the silo side-wall, and the inner pipe is welded on the outer pipe-wall and connected to a large elbow. In this paper, we assume both the inner and outer concentric pipes are fixed at the inlet end. It has been discovered that the turbulent mixing of jets coming out of the concentric pipes before the fan pump contributes significantly to the smooth operation of impellers, the uniformity of stock consistency, and the minimization of pressure variations (Wang *et al.* 1999). In addition, the turbulent jets may introduce strong oscillations in the suspended pipes, which can cause structural damage, such as fatigue failure of pipe joints. Therefore, in a proper silo–pipe system design, vibration problems associated with such pipes must be understood and resovled.

In this paper, we consider vibration issues that relate directly to the design of the silo mixing unit, and leave the static and dynamic stability analyses to a forthcoming paper (Wang & Bloom 1999). The basic goal of this work is to determine the protruded inner tubular pipe oscillation frequency and damping ratio resulting from both internal and external fluid flows. Considering the fact that the inner pipe carries thick fiber stock and has a much smaller diameter than the outer pipe, we shall focus exclusively on the inner pipe vibration and address the following issues: (i) what is the frequency range for a given pipe system design; (ii) what is the effect of the angle of inclination; (iii) what is the optimal

0889–9746/99/040443 + 18 $30.00

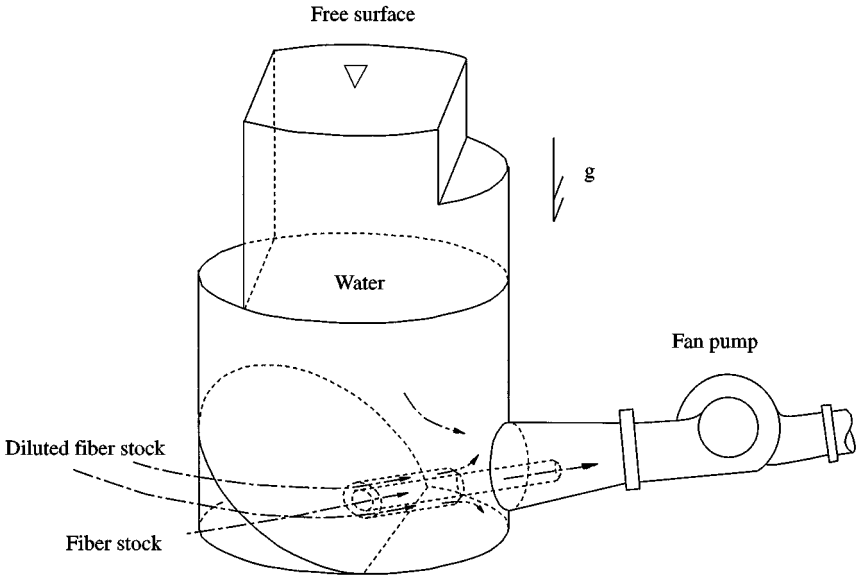

Figure 1. Location of the mixing pipe in the silo unit.

choice of pipe flow velocities and radii; (iv) what are the critical lengths of the pipes; and (v) how important is the depth of the submerged pipe system.

The problem analyzed in this paper belongs to a major subject area within the general realm of fluid–structure interaction problems. The study of flow-induced vibrations and stability of pipes has a long history, beginning with the work of Benjamin (1961a, b) and Païdoussis (1966a, b). A recent survey of the subject is available in Paidoussis & Li (1993).

The main objective of this paper is to propose a mathematical model for inclined, submerged, concentric pipes with different pipe lengths. In this model, the fluid forces exerted by both the confined and unconfined external flows are considered. We start with the derivation of the governing equations of motion in Section 2, and discuss finite-difference schemes for spatial discritizations in Section 3. Finally, we present, in Section 4 numerical examples for a typical pipe system design along with an analysis to determine critical design parameters.

2. GOVERNING EQUATIONS OF MOTION

A schematic diagram of the location and general configuration of the mixing pipe arrangement within the silo is shown in Figure 1. As depicted in Figure 2, the mathematical model of the suspended concentric pipes includes the inner pipe with a length l and the outer pipe with a length $L < l$. We note that all the pipes are submerged in silo water, and that continuous flow between the two concentric cylinders only occurs in the domain $0 \leq x \leq L$. Under the action of the gravitational force and fluid forces, i.e. pressure and frictional forces, the inner pipe will deform and oscillate.

Using the small displacement and small strain assumptions, the body coordinates (ξ, η, ζ), corresponding to the deformed configuration, can be projected onto the initial coordinates

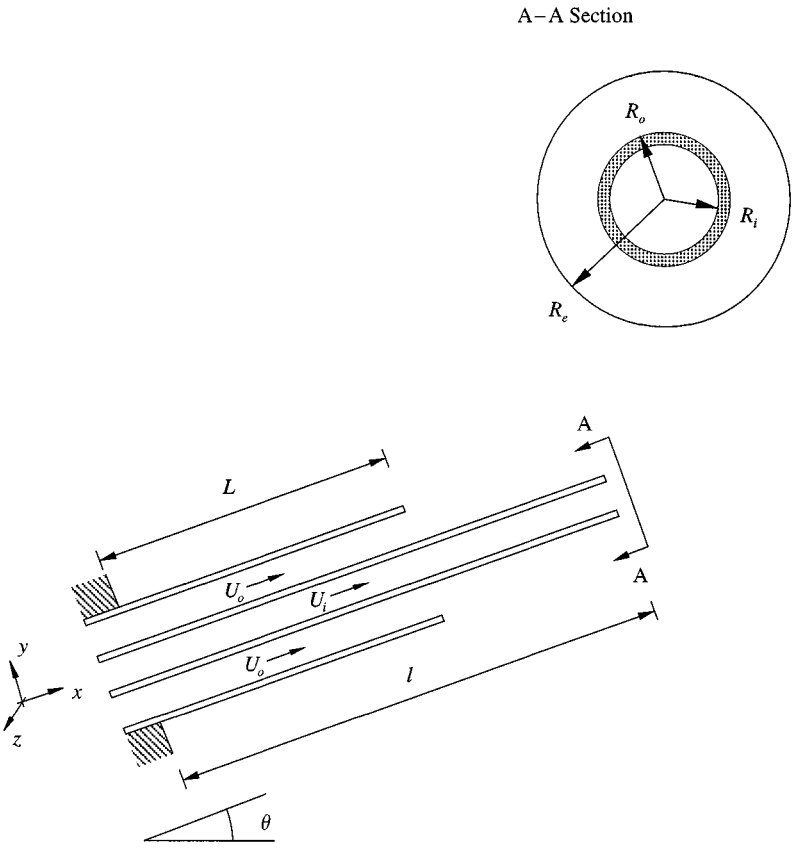

Figure 2. The concentric piping equilibrium configuration.

(x, y, z), as shown in Figure 3, with the following results:

$$\xi_x \simeq \xi, \quad \xi_y \simeq \xi \frac{\partial y}{\partial x}, \quad \xi_z \simeq \xi \frac{\partial z}{\partial x},$$

$$\eta_x \simeq -\eta \frac{\partial y}{\partial x}, \quad \eta_y \simeq \eta, \quad \eta_z \simeq 0, \tag{1}$$

$$\zeta_x \simeq -\zeta \frac{\partial z}{\partial x}, \quad \zeta_y \simeq 0, \quad \zeta_z \simeq \zeta,$$

where the in-plane (x-y plane) and out-of-plane displacements are denoted as $y = y(x, t)$ and $z = z(x, t)$.

In this paper, we establish the force equilibrium on the deformed configurations in order to retain certain nonlinear terms at the beginning of our derivation. Nevertheless, we shall focus on the linear vibration analysis and leave the nonlinear analysis of the subject to a forthcoming paper.

We consider that fluid flows within the inner tube and the concentric region between the inner and outer pipes are fully developed turbulent flows, and express the forces exerted on the inner tubular beam from the internal and external fluid flows as $(F^i_\xi, F^i_\eta, F^i_\zeta)$ and

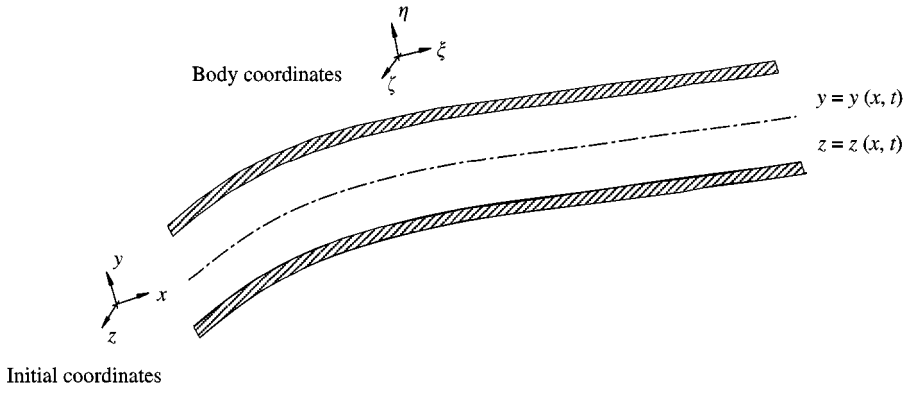

Figure 3. Deformed element of the inner tubular beam.

$(F^e_\xi, F^e_\eta, F^e_\zeta)$, respectively. As a consequence of equation (1), we may project the internal fluid forces on the initial coordinates (x, y, z) as follows:

$$(F^i_\xi)_x \simeq F^i_\xi, \quad (F^i_\xi)_y \simeq F^i_\xi \frac{\partial y}{\partial x}, \quad (F^i_\xi)_z \simeq F^i_\xi \frac{\partial z}{\partial x},$$

$$(F^i_\eta)_x \simeq -F^i_\eta \frac{\partial y}{\partial x}, \quad (F^i_\eta)_y \simeq F^i_\eta, \quad (F^i_\eta)_z \simeq 0, \tag{2}$$

$$(F^i_\zeta)_x \simeq -F^i_\zeta \frac{\partial z}{\partial x}, \quad (F^i_\zeta)_y \simeq 0, \quad (F^i_\zeta)_z \simeq F^i_\zeta,$$

and similar projections can be obtained with respect to the external fluid forces.

We denote by R_i the inner radius of the internal pipe; therefore, the internal fluid occupies a domain with cross-sectional area $A_i = \pi R_i^2$. We also let R_o and R_e denote the outer radius of the internal pipe and the inner radius of the external pipe. In addition, we assign ρ_i and ρ_e, U_i and U_e to be the fluid densities, constant averaged turbulent flow velocities for the internal and external regions.

We initiate our derivation of the governing equations for $y(x, t)$ and $z(x, t)$ by writting down the force equilibrium for the inner tubular beam, which has flexural rigidity EI, where E is the Young's modulus, and I, expressed as $I = \pi(R_o^4 - R_i^4)/4$, is the moment of inertia of the tubular beam cross-sectional area.

As depicted in Figure 4, a differential element $\mathrm{d}x$ of the beam is acted upon by forces due to gravity g with an inclination angle θ, tension T, fluid forces $(F^i_\xi, F^i_\eta, F^i_\zeta)$ and $(F^e_\xi, F^e_\eta, F^e_\zeta)$, and transverse shear forces (Q_y, Q_z). Following Hannoyer & Païdoussis (1978), in the present analysis we discount the influence of any moments that may be exerted by the internal and external flows. Also depicted in Figure 4 are the bending moments M_y and M_z in accord with $y(x, t)$ and $z(x, t)$. In the standard manner, if we ignore viscoelastic damping effects and consider the beam as an Euler–Bernoulli beam with constant cross-sectional area, the bending moments, M_y and M_z, and the shear forces, Q_y and Q_z take on the form

$$M_y = EI \frac{\partial^2 y}{\partial x^2}, \quad Q_y = -EI \frac{\partial^3 y}{\partial x^3},$$

$$M_z = EI \frac{\partial^2 z}{\partial x^2}, \quad Q_z = -EI \frac{\partial^3 z}{\partial x^3}. \tag{3}$$

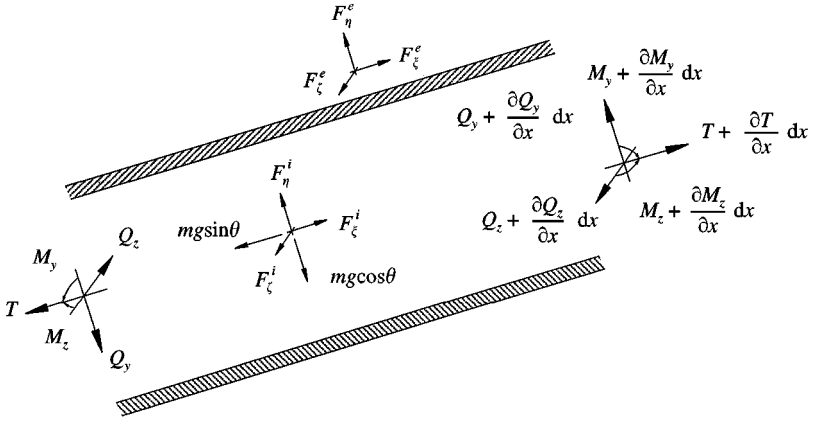

Figure 4. Forces acting on a differential element of the inner tubular beam.

Therefore, we ignore the axial inertia effect, and derive the governing equations for the tubular beam as

$$\frac{\partial T}{\partial x} + \left(F_\xi^i - F_\eta^i \frac{\partial y}{\partial x} - F_\zeta^i \frac{\partial z}{\partial x}\right) + \left(F_\xi^e - F_\eta^e \frac{\partial y}{\partial x} - F_\zeta^e \frac{\partial z}{\partial x}\right) - \frac{\partial}{\partial x}\left(Q_y \frac{\partial y}{\partial x}\right) - \frac{\partial}{\partial x}\left(Q_z \frac{\partial z}{\partial x}\right) - mg\sin\theta = 0, \tag{4}$$

$$\frac{\partial}{\partial x}\left(T \frac{\partial y}{\partial x}\right) + \frac{\partial Q_y}{\partial x} + \left(F_\eta^i + F_\xi^i \frac{\partial y}{\partial x}\right) + \left(F_\eta^e + F_\xi^e \frac{\partial y}{\partial x}\right) = m \frac{\partial^2 y}{\partial t^2} + mg\cos\theta, \tag{5}$$

$$\frac{\partial}{\partial x}\left(T \frac{\partial z}{\partial x}\right) + \frac{\partial Q_z}{\partial x} + \left(F_\zeta^i + F_\xi^i \frac{\partial z}{\partial x}\right) + \left(F_\zeta^e + F_\xi^e \frac{\partial z}{\partial x}\right) = m \frac{\partial^2 z}{\partial t^2}, \tag{6}$$

where m denotes the mass per unit length of the tubular beam.

Furthermore, from the force equilibrium for the internal flow [see, for example, Hannoyer & Païdoussis (1979), Païdoussis (1970) and Païdoussis & Pettigrew (1979)], we can express the internal fluid forces as follows:

$$F_\xi^i - F_\eta^i \frac{\partial y}{\partial x} - F_\zeta^i \frac{\partial z}{\partial x} = -\frac{\partial}{\partial x}(p_i A_i) - \rho_i A_i g \sin\theta, \tag{7}$$

$$F_\eta^i + F_\xi^i \frac{\partial y}{\partial x} = -\frac{\partial}{\partial x}\left(p_i A_i \frac{\partial y}{\partial x}\right) - \rho_i A_i g\cos\theta - \rho_i A_i \left(\frac{\partial}{\partial t} + U_i \frac{\partial}{\partial x}\right)^2 y, \tag{8}$$

$$F_\zeta^i + F_\xi^i \frac{\partial z}{\partial x} = -\frac{\partial}{\partial x}\left(p_i A_i \frac{\partial z}{\partial x}\right) - \rho_i A_i \left(\frac{\partial}{\partial t} + U_i \frac{\partial}{\partial x}\right)^2 z. \tag{9}$$

Finally, we turn our attention to the contributions from the external fluid flow. We treat the external flow a little differently because of the fact that we can no longer directly replace the forces acting on the outer surface of the inner pipe with the equivalent flow pressure, inertia, and gravitational forces. We note that we have two different regions to consider, i.e. the confined region $0 \le x < L$ and the unconfined region $L \le x \le l$. However, due to the outlet opening at the location $x = L$, the hydrostatic pressure is continuous in both regions, and for the tubular beam with a uniform cross-sectional area, the components of the

net forces attributable to the external hydrostatic and hydrodynamic fluid pressures are given by

$$\mathscr{F}_x^1 = 0,$$
$$\mathscr{F}_y^1 = \rho_e A_o g \cos\theta + \frac{\partial}{\partial x}\left((p_e + p_o) A_o \frac{\partial y}{\partial x}\right), \tag{10}$$
$$\mathscr{F}_z^1 = \frac{\partial}{\partial \mathrm{x}}\left((p_e + p_o) A_o \frac{\partial z}{\partial x}\right),$$

where p_e and p_o stand for the hydrostatic and hydrodynamic pressures, respectively, and the cross-sectional area A_o is defined as πR_o^2. By denoting the free-surface level measured from the origin (0, 0, 0) as y_o, such that the hydrostatic pressure at the tip of the submerged beam ($x = l$) is given by $\bar{p} = \rho_e g y_o - \rho_e g l \sin\theta$, we obtain the expression for the hydrostatic pressure of the external fluid,

$$p_e = (l - x)\rho_e g \sin\theta - \mathrm{y}\rho_e \mathrm{g}\cos\theta + \bar{p}. \tag{11}$$

Moreover, according to Hannoyer & Païdoussis (1978), Païdoussis (1973) and Païdoussis & Pettigrew (1979), we have the following expression for the hydrodynamic pressure in the concentric flow region:

$$p_o A_o = \tfrac{1}{2}\rho_e D_o U_e^2 C_f h(x), \tag{12}$$

where the friction coefficient C_f has, according to Païdoussis (1966a, b), Schlichting (1987) and Taylor (1952), different values in the confined and unconfined regions,

$$C_f = \begin{cases} C_f^1, & 0 \le x < L, \\ C_f^2, & L \le x \le l \end{cases} \tag{13}$$

and

$$h(x) = \begin{cases} \dfrac{D_o}{D_e - D_o}(L - x), & 0 \le x < L, \\ 0, & L \le x \le l, \end{cases} \tag{14}$$

along with

$$\frac{\mathrm{d}h(x)}{\mathrm{d}x} = \begin{cases} -\dfrac{D_o}{D_e - D_o}, & 0 \le x < L, \\ 0, & L \le x \le l. \end{cases} \tag{15}$$

As discussed in Hannoyer & Païdoussis (1979) and Païdoussis (1966, 1973), the external flow exerts on the tubular beam the following viscous forces per unit length in both the normal (η, ζ) and longitudinal (ξ) directions:

$$f_\xi^e = \tfrac{1}{2}\rho_e D_o U_e^2 C_f,$$
$$f_\eta^e = -\tfrac{1}{2}\rho_e D_o U_e C_f \left(\frac{\partial y}{\partial t} + U_e \frac{\partial y}{\partial x}\right), \tag{16}$$
$$f_\zeta^e = -\tfrac{1}{2}\rho_e D_o U_e C_f \left(\frac{\partial z}{\partial t} + U_e \frac{\partial z}{\partial x}\right),$$

where D_o is outer diameter of the inner pipe.

Turning now to the fluid inertia forces, we take x_o to be the entrance distance associated with the turbulent boundary layer, define the functions $\sigma = 1 + 0{\cdot}4(x_o/L)C_f^1$ and

$\alpha = 0{\cdot}4\,C_f^1/\sigma$ for the confined external flow region, and introduce for the components of the inertia forces

$$\mathscr{F}_x^2 = 0,$$

$$\mathscr{F}_y^2 = -\chi\rho_e A_o\left(\frac{\partial}{\partial t} + \tilde{U}_e\frac{\partial}{\partial x}\right)\left(\frac{\partial}{\partial t} + U_e\frac{\partial}{\partial x}\right)y, \tag{17}$$

$$\mathscr{F}_z^2 = -\chi\rho_e A_o\left(\frac{\partial}{\partial t} + \tilde{U}_e\frac{\partial}{\partial x}\right)\left(\frac{\partial}{\partial t} + U_e\frac{\partial}{\partial x}\right)z,$$

where

$$\chi = \begin{cases} \dfrac{R_e^2 + R_o^2}{R_e^2 - R_o^2}, & 0 \le x < L, \\ 1, & L \le x \le l \end{cases} \tag{18}$$

and

$$\tilde{U}_e = \begin{cases} U_e(1 - \alpha(x/L)^2)/\sigma, & 0 \le x < L, \\ U_e, & L \le x \le l. \end{cases} \tag{19}$$

Therefore, the overall external fluid forces are written as

$$F_\xi^e - F_\eta^e\frac{\partial y}{\partial x} - F_\zeta^e\frac{\partial z}{\partial x} = \mathscr{F}_x^1 + \left(f_\xi^e - f_\eta^e\frac{\partial y}{\partial x} - f_\zeta^e\frac{\partial z}{\partial x}\right) + \mathscr{F}_x^2, \tag{20}$$

$$F_\eta^e + F_\xi^e\frac{\partial y}{\partial x} = \mathscr{F}_y^1 + \left(f_\eta^e + f_\xi^e\frac{\partial y}{\partial x}\right) + \mathscr{F}_y^2, \tag{21}$$

$$F_\zeta^e + F_\xi^e\frac{\partial z}{\partial x} = \mathscr{F}_z^1 + \left(f_\zeta^e + f_\xi^e\frac{\partial z}{\partial x}\right) + \mathscr{F}_z^2. \tag{22}$$

From this point on, we shall ignore all nonlinear terms that appear in the three sets of force balance equations, as a consequence of the small displacement and small strain assumptions. The key point in simplifying the governing equations (4)–(6) is to obtain the explicit expression for the tension T, based on the assumption $p_i|_{x=l} = \bar{p} - \frac{1}{2}\rho_e D_o^2 U_e^2 C_b/A$, and the axial force equilibrium at the tip of the tubular beam, i.e. $T|_{x=l} = -\bar{p}A + \frac{1}{2}\rho_e D_o^2 U_e^2 C_b$, where A denotes the cross-sectional area of the tubular beam, which is given by $\pi(R_o^2 - R_i^2)$, and C_b is the coefficient representing the base drag. Thus, if the tubular beam density is ρ, the mass per unit length m can be expressed as ρA. Abbreviating $-\bar{p}A_o + \frac{1}{2}\rho_e D_o^2 U_e^2 C_b A_o/A$ as $\mathscr{G}_0$, $(m + \rho_i A_i)g\sin\theta$ as $\mathscr{G}_1$, and $\frac{1}{2}\rho_e D_o U_e^2$ as $\mathscr{G}_2$, we obtain from equations (4), (7) and (20)

$$\frac{\partial(T - p_i A_i)}{\partial x} = \mathscr{G}_1 - \mathscr{G}_2 C_f, \tag{23}$$

so that

$$\begin{aligned} T - p_i A_i &= \mathscr{G}_0 + (x - l)\mathscr{G}_1 + \mathscr{G}_2\int_x^l C_f\,\mathrm{d}x \\ &= \mathscr{G}_0 + (x - l)\mathscr{G}_1 + \mathscr{G}_2\begin{cases} C_f^1(L - x) + C_f^2(l - L), & 0 \le x < L, \\ C_f^2(l - x), & L \le x \le l. \end{cases} \end{aligned} \tag{24}$$

Using, respectively, the sets of equations (5), (8) and (21), and (6), (9) and (22), it is now an easy task to derive the following governing linearized equations:

$$C_1 \frac{\partial^4 y}{\partial x^4} + C_2 \frac{\partial^2 y}{\partial x^2} + C_3 \frac{\partial^2 y}{\partial x \partial t} + C_4 \frac{\partial^2 y}{\partial t^2} + C_5 \frac{\partial y}{\partial x} + C_6 \frac{\partial y}{\partial t} + C_7 = 0, \tag{25}$$

$$D_1 \frac{\partial^4 z}{\partial x^4} + D_2 \frac{\partial^2 z}{\partial x^2} + D_3 \frac{\partial^2 z}{\partial x \partial t} + D_4 \frac{\partial^2 z}{\partial t^2} + D_5 \frac{\partial z}{\partial x} + D_6 \frac{\partial z}{\partial t} + D_7 = 0, \tag{26}$$

where the two sets of coefficients are given by

$$\begin{aligned}
C_1 &= EI, \\
C_2 &= \rho_i A_i U_i^2 - (T - p_i A_i + p_e A_o + \tfrac{1}{2}\rho_e D_o U_e^2 C_f h(x)) + \chi \rho_e A_o \tilde{U}_e U_e, \\
C_3 &= 2\rho_i A_i U_i + \chi \rho_e A_o (U_e + \tilde{U}_e), \\
C_4 &= m + p_i A_i + \chi \rho_e A_o, \\
C_5 &= -(m + p_i A_i - \rho_e A_o) g \sin\theta + \tfrac{1}{2}\rho_e D_o U_e^2 C_f \left(1 - \frac{\mathrm{d}h(x)}{\mathrm{d}x}\right), \\
C_6 &= \tfrac{1}{2}\rho_e D_o U_e C_f, \\
C_7 &= (m + \rho_i A_i - \rho_e A_o) g \cos\theta;
\end{aligned} \tag{27}$$

and

$$\begin{aligned}
D_1 &= EI, \\
D_2 &= \rho_i A_i U_i^2 - (T - p_i A_i + p_e A_o + \tfrac{1}{2}\rho_e D_o U_e^2 C_f h(x)) + \chi \rho_e A_o \tilde{U}_e U_e, \\
D_3 &= 2\rho_i A_i U_i + \chi \rho_e A_o (U_e + \tilde{U}_e), \\
D_4 &= m + p_i A_i + \chi \rho_e A_o, \\
D_5 &= -(m + p_i A_i - \rho_e A_o) g \sin\theta + \tfrac{1}{2}\rho_e D_o U_e^2 C_f \left(1 - \frac{\mathrm{d}h(x)}{\mathrm{d}x}\right), \\
D_6 &= \tfrac{1}{2}\rho_e D_o U_e C_f, \\
D_7 &= 0.
\end{aligned} \tag{28}$$

Remark I. For the clamped (or built-in) boundary condition at $x = 0$, we have

$$\begin{aligned}
y(0, t) = 0, \quad \frac{\partial y(0, t)}{\partial x} = 0, \\
z(0, t) = 0, \quad \frac{\partial z(0, t)}{\partial x} = 0,
\end{aligned} \tag{29}$$

while for the free end of the tubular beam at $x = l$, we have

$$\begin{aligned}
\frac{\partial^2 y(l, t)}{\partial x^2} = 0, \quad EI \frac{\partial^3 y(l, t)}{\partial x^3} + \left(\bar{p}A - \frac{1}{2}\rho_e D_o^2 U_e^2 C_b\right) \frac{\partial y(l, t)}{\partial x} = 0, \\
\frac{\partial^2 z(l, t)}{\partial x^2} = 0, \quad EI \frac{\partial^3 z(l, t)}{\partial x^3} + \left(\bar{p}A - \frac{1}{2}\rho_e D_o^2 U_e^2 C_b\right) \frac{\partial z(l, t)}{\partial x} = 0.
\end{aligned} \tag{30}$$

Remark II. We recognize that the coefficients C_2 to C_6 and D_2 to D_6 are variables depending on the position x. To circumvent the discontinuity at the location $x = L$, where the confined and unconfined domains are separated, we prescribe a nodal point at that location.

Remark III. By neglecting nonlinear terms, the governing equations for $y(x, t)$ and $z(x, t)$ turn out to be decoupled. In addition, we notice that the only difference between equations (25) and (26) occurs in the inhomogeneous terms C_7 and D_7. However, such a difference will not affect the linear dynamic analysis based on the characteristic equations. Therefore, from here on, we shall deal exclusively with equation (25).

Remark IV. Because of the small displacement and small strain assumptions, we may ignore the contribution of the term involving y and rewrite the expression for the hydrostatic pressure of the external fluid, equation (11), as

$$p_e \simeq (l - x)\rho_e g \sin\theta + \bar{p}. \tag{31}$$

3. NUMERICAL ANALYSIS

Considering the fact that we have third- and fourth-order spatial derivatives in equation (25), standard C^0 finite elements cannot be used. An elaborate discussion on the use of C^1 finite elements or mixed formulations is available in Bathe (1996) and Zienkiewicz (1977). In this paper, we employ the method of finite differences to replace the partial differential equation (25) with a set of ordinary differential equations with respect to time. Equivalent difference schemes are also used for the boundary conditions in equations (29) and (30). We define the solution variable $y(x, t)$ at the spatial grid (or nodal) point i as $Y^i(t)$ (depicted in Figure 5), and its corresponding time derivative as $\dot{Y}^i(t)$. Using an equal spacing h between finite-difference stations, we obtain the following finite-difference approximation for various differentiations:

$$\begin{aligned}
\left.\frac{\partial y}{\partial x}\right|_i &= \frac{Y^{i+1} - Y^{i-1}}{2h},\\
\left.\frac{\partial^2 y}{\partial x^2}\right|_i &= \frac{Y^{i+1} - 2Y^i + Y^{i-1}}{h^2},\\
\left.\frac{\partial^3 y}{\partial x^3}\right|_i &= \frac{Y^{i+2} - 2Y^{i+1} + 2Y^{i-1} - Y^{i-2}}{2h^3},\\
\left.\frac{\partial^4 y}{\partial x^4}\right|_i &= \frac{Y^{i+2} - 4Y^{i+1} + 6Y^i - 4Y^{i-1} + Y^{i-2}}{h^4}.
\end{aligned} \tag{32}$$

In addition, by employing the same finite-difference procedure, we obtain from the boundary conditions in equations (29) and (30)

$$\begin{aligned}
Y^0 &= 0,\\
Y^{-1} &= Y^1\\
Y^{N+1} &= 2Y^N - Y^{N-1},\\
Y^{N+2} &= \left(4 - \frac{(2\bar{p}A - \rho_e D_o^2 U_e^2 C_b)h^2}{EI}\right)(Y^N - Y^{N-1}) + Y^{N-2}.
\end{aligned} \tag{33}$$

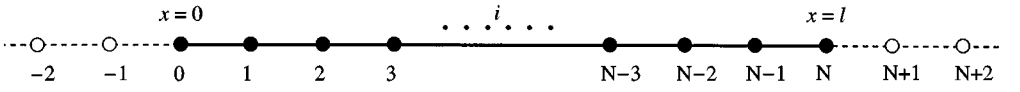

Figure 5. Finite difference stations on the tubular beam.

Therefore, the discretized characteristic equation based on the equilibrium equation (25) can be written as follows, for node $i (1 \leq i \leq N)$:

$$C_4^i \ddot{Y}^i + \frac{C_3^i}{2h} \dot{Y}^{i+1} + C_6^i \dot{Y}^i - \frac{C_3^i}{2h} \dot{Y}^{i-1} + \frac{C_1^i}{h^4} Y^{i+2} + \left(\frac{C_2^i}{h^2} - \frac{4C_1^i}{h^4} + \frac{C_5^i}{2h} \right) Y^{i+1}$$
$$+ \left(\frac{6C_1^i}{h^4} - \frac{2C_2^i}{h^2} \right) Y^i + \left(\frac{C_2^i}{h^2} - \frac{4C_1^i}{h^4} - \frac{C_5^i}{2h} \right) Y^{i-1} + \frac{C_1^i}{h^4} Y^{i-2} = 0. \tag{34}$$

Note that the variable coefficients C_1 to C_6 in equation (27) are functions of x and are denoted as C_1^i to C_6^i at the nodal point i. Moreover, substituting equation (33) into (34) gives

$$\mathbf{M}\ddot{\mathbf{Y}} + \mathbf{C}\dot{\mathbf{Y}} + \mathbf{K}\mathbf{Y} = \mathbf{0}, \tag{35}$$

where $\mathbf{Y}$ is the solution vector, and $\mathbf{M}$, $\mathbf{C}$ and $\mathbf{K}$ stand for the mass, damping (including gyroscopic terms) and stiffness algebraic coefficient matrices, respectively. For the practical geometries (discussed in detail in the following section), the gyroscopic term governed by C_3 is much more significant than the frictional damping term C_6, while C_1 is the predominant stiffness term. Having the set of second-order ordinary differential equations in equation (35), we can then assume a characteristic solution $\mathbf{Y} = e^{i\omega t}\hat{\mathbf{Y}}$, where $\hat{\mathbf{Y}}$ is the mode shape corresponding to the natural frequency of the coupled system $\omega = 2\pi f$, and employ standard eigenvalue solution techniques. Of course, $\mathscr{R}e(f)$ corresponds to the true resonant frequency, and $\mathscr{I}m(f)$ represents the damping. The extensive account of the positive $\mathscr{I}m(f)$ part and other stability issues will be discussed in Wang & Bloom (1999).

4. RESULTS

To find the frequency range of a particular pipe system design, we model one system currently used in the paper industry with the following physical parameters: $\rho_i = \rho_e = 1000$ kg/m^3; $\rho = 7800$ kg/m^3; $l = 2{\cdot}392$ m; $L = 1{\cdot}135$ m; $x_o = 2{\cdot}4$ m; $y_o = 6{\cdot}155$ m; $R_i = 0{\cdot}1165$ m; $R_o = 0{\cdot}1397$ m; $R_e = 0{\cdot}2096$ m; $g = 9{\cdot}8$ m/s^2; $C_f^1 = 0{\cdot}004\pi$; $C_f^2 = 0{\cdot}5\pi R_i/l$; $C_b = 0{\cdot}0125\pi$; $E = 200$ GPa; $U_i = 2$ m/s; and $U_e = 1$ m/s. In order to evaluate the friction coefficients, we need to calculate the Reynolds number defined as $\mathscr{R}e = ua/v$, where a is a characteristic length, such as one of the pipe diameters in this case; u is a characteristic flow velocity, such as U_i and U_e; and v stands for the kinematic viscosity; in this work, we use $v = 1{\cdot}13226 \times 10^{-6}$ m^2/s. Notice that when $\mathscr{R}e < 10^4$, the friction coefficients as well as the viscosity of the fiber–water mixture can be significantly different from those of the pure water (Daily & Bugliarello 1961).

For the particular configuration described above, we find that

$$\text{with coupling:} \quad f_1 = 34{\cdot}15 + 0{\cdot}08467\text{i Hz}, \quad f_2 = 201{\cdot}0 + 0{\cdot}09622\text{i Hz};$$

$$\text{without coupling:} \quad f_1 = 45{\cdot}04 + 0\text{i Hz}, \quad f_2 = 282{\cdot}3 + 0\text{i Hz}.$$

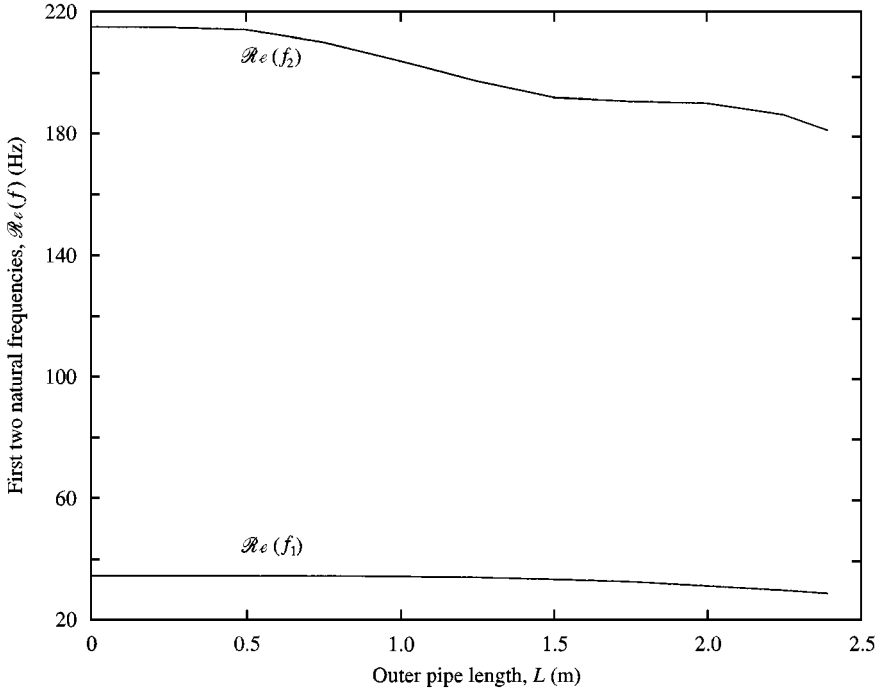

Figure 6. First two coupled system frequencies versus the outer pipe length L (42 grid points with fixed inner pipe length $l = 2{\cdot}392$ m).

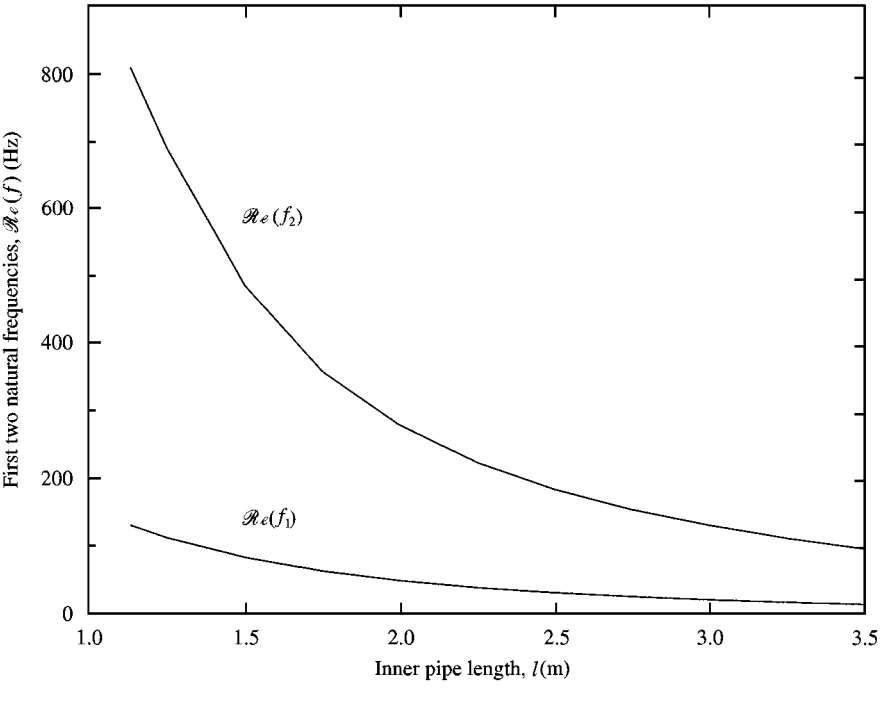

Figure 7. First two coupled system frequencies versus the inner pipe length l (42 grid points with fixed outer pipe length $L = 1{\cdot}135$ m).

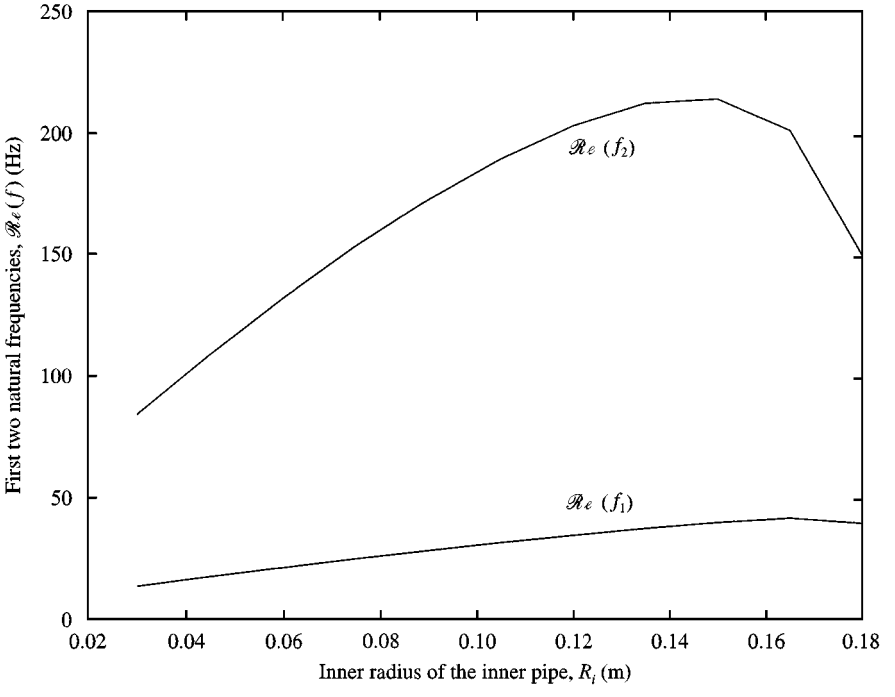

Figure 8. First two coupled system frequencies versus the inner radius of the inner pipe R_i (42 grid points with fixed inner pipe wall thickness $R_o - R_i = 0{\cdot}0232$ m).

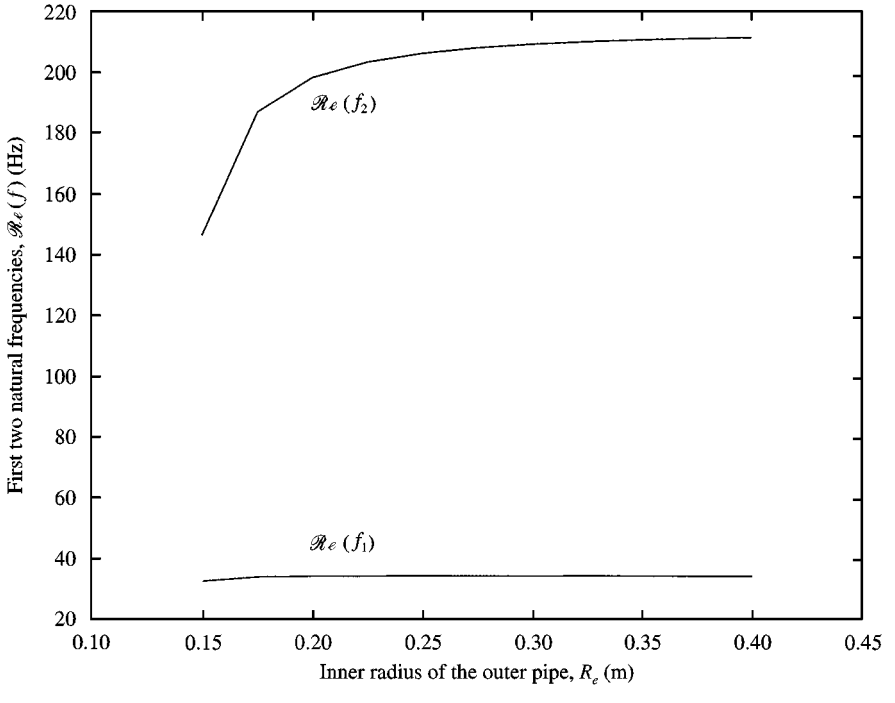

Figure 9. First two coupled system frequencies versus the inner radius of the outer pipe R_e (42 grid points).

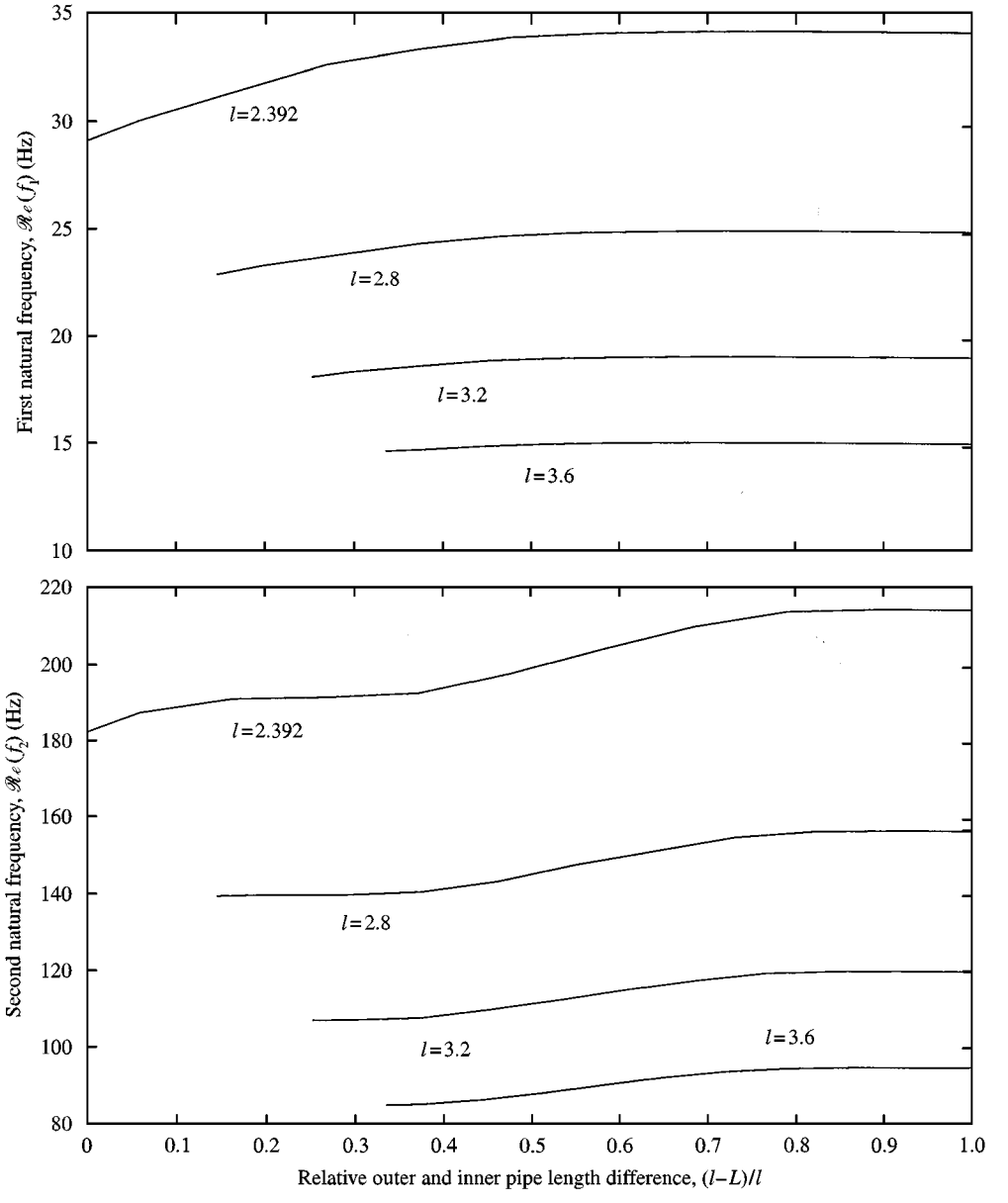

Figure 10. First two coupled system frequencies versus relative outer and inner pipe length difference $(l - L)/l$ (42 grid points).

The analytical solutions for the natural frequencies of the cantilever beam without coupling to the surrounding fluids are expressed as $f_i = (\lambda_i^2/2\pi l^2)\sqrt{EI/m}$, $i = 1, 2, 3, \ldots$, where λ_i are constants listed, for instance, in Blevins (1979). In addition to the introduction of damping effects, the interaction between the inner tubular beam and the internal and external fluids significantly diminish the natural frequencies.

To come up with critical design criteria concerning the dynamical behavior of the tubular beam, we need to vary the pipe lengths, inclination angle, free surface level, flow velocities, and pipe radii. We shall hold in this paper, as it is done in practice, the volume flow rates

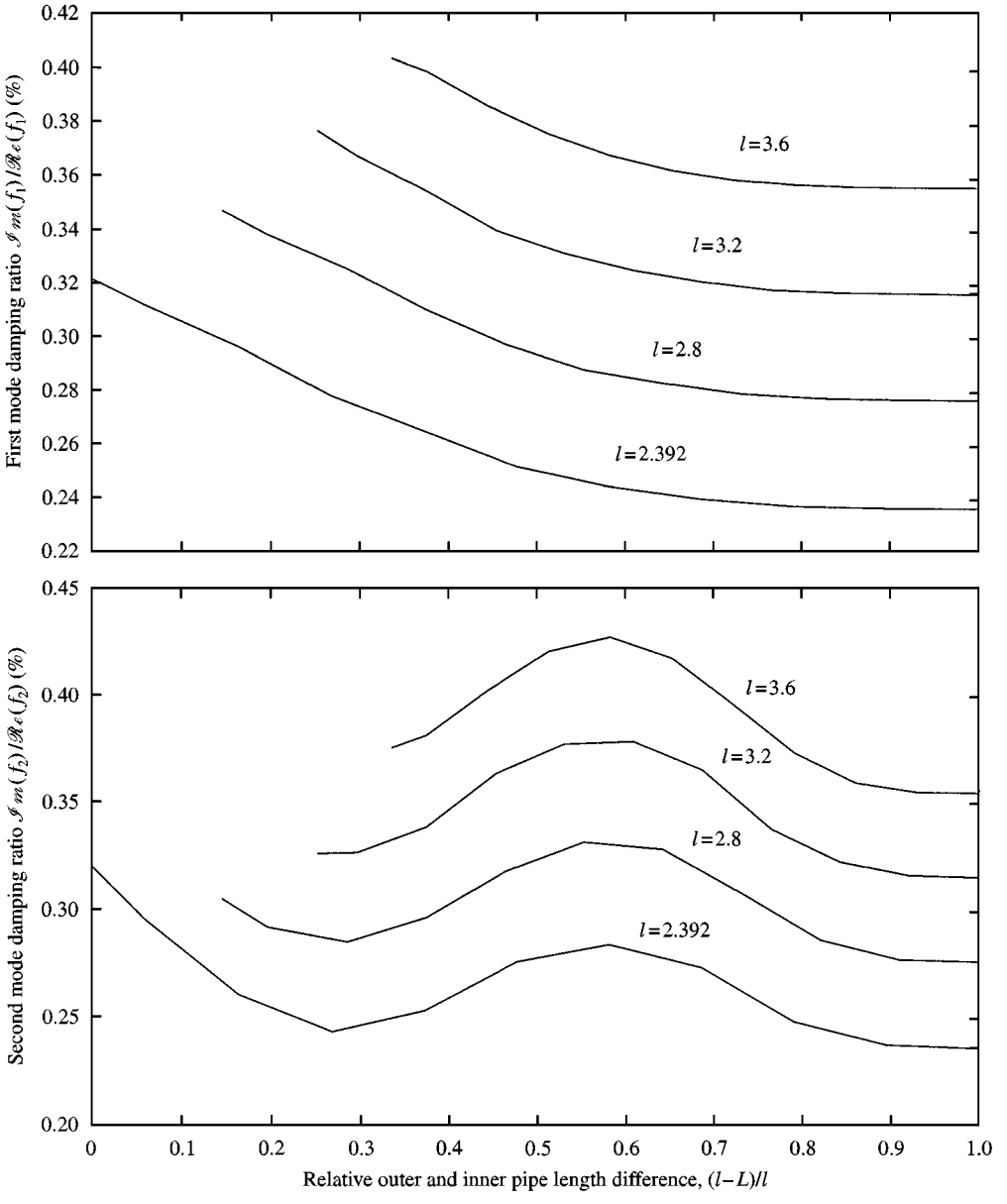

Figure 11. Damping ratio of the first two coupled system frequencies versus relative outer and inner pipe length difference $(l - L)/l$ (42 grid points).

constant to $8{\cdot}5277 \times 10^{-2}$ m^3/s for the internal flow, and to $7{\cdot}6705 \times 10^{-2}$ m^3/s for the external flow. In other words, if we reduce the inner pipe radius, the inner fluid flow velocity will increase accordingly, and *vice versa*; the same is true for the outer pipe. In addition, with a constant free surface level, the external hydrostatic pressure p_e will vary in accordance with the inner pipe length and the inclination angle. Finally, we vary y_o, which governs the depth of the immersed pipe system. However, we recognize that a design parameter such as y_o is often related to the fan-pump pressure drop and, in practice, cannot be modified easily.

Figure 6 shows the first two coupled frequencies of the fluid–structure system $\mathscr{R}e(f_1)$ and $\mathscr{R}e(f_2)$ for various outer pipe lengths. As can be seen, the longer the outer pipe, the smaller are the natural frequencies of the inner pipe, i.e. the increased confinement of the inner pipe increases its effective (fluid added) mass. In Figure 7, we observe that varying the inner pipe length has a similar, however, much stronger effect on the coupled system frequencies. The physical explanation is that the inner pipe length determines directly the inner pipe structural stiffness and mass (in fact, for a cantilever beam, the natural frequency is inversely proportional to the square of the beam length), and the outer pipe length only

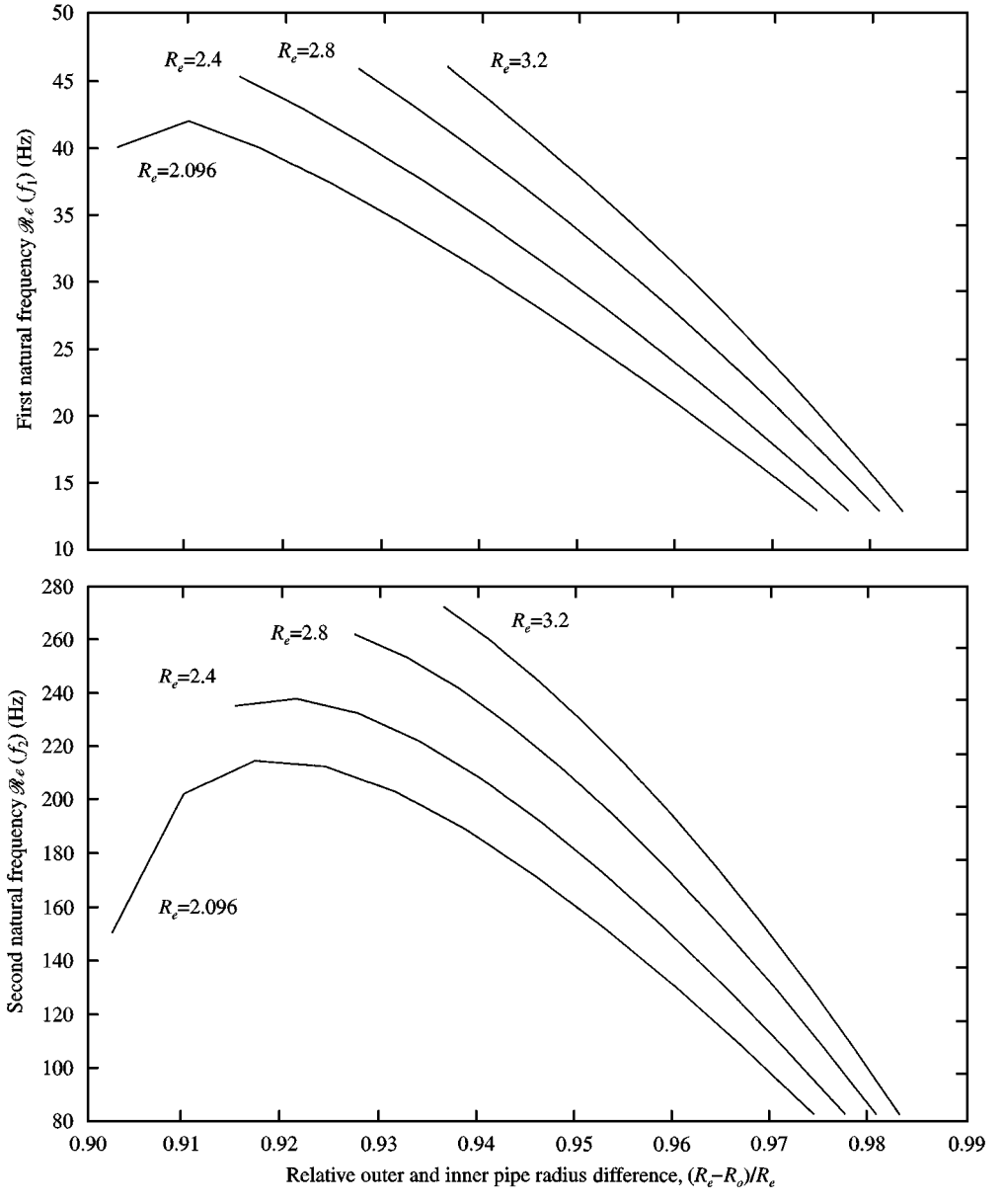

Figure 12. First two coupled system frequencies versus relative outer and inner pipe radius difference $(R_e - R_o)/R_e$ (42 grid points).

contributes to the fluid–structure coupling part. In general, if the structure is more flexible, it is more susceptible to turbulence buffeting as well as to buckling or flutter. Figures 6 and 7 also show that the coupled system frequencies for the given design configuration with different pipe lengths are between the lower and upper bounds calculated for the two cases in which the inner and outer pipes have the same lengths of l and L, respectively.

In addition, we find in Figures 6 and 7 that the lengths of the pipes have a much larger effect on the second coupled system natural frequency than the first one. This result also matches the physical understanding based on the dependence of mode shapes on the pipe

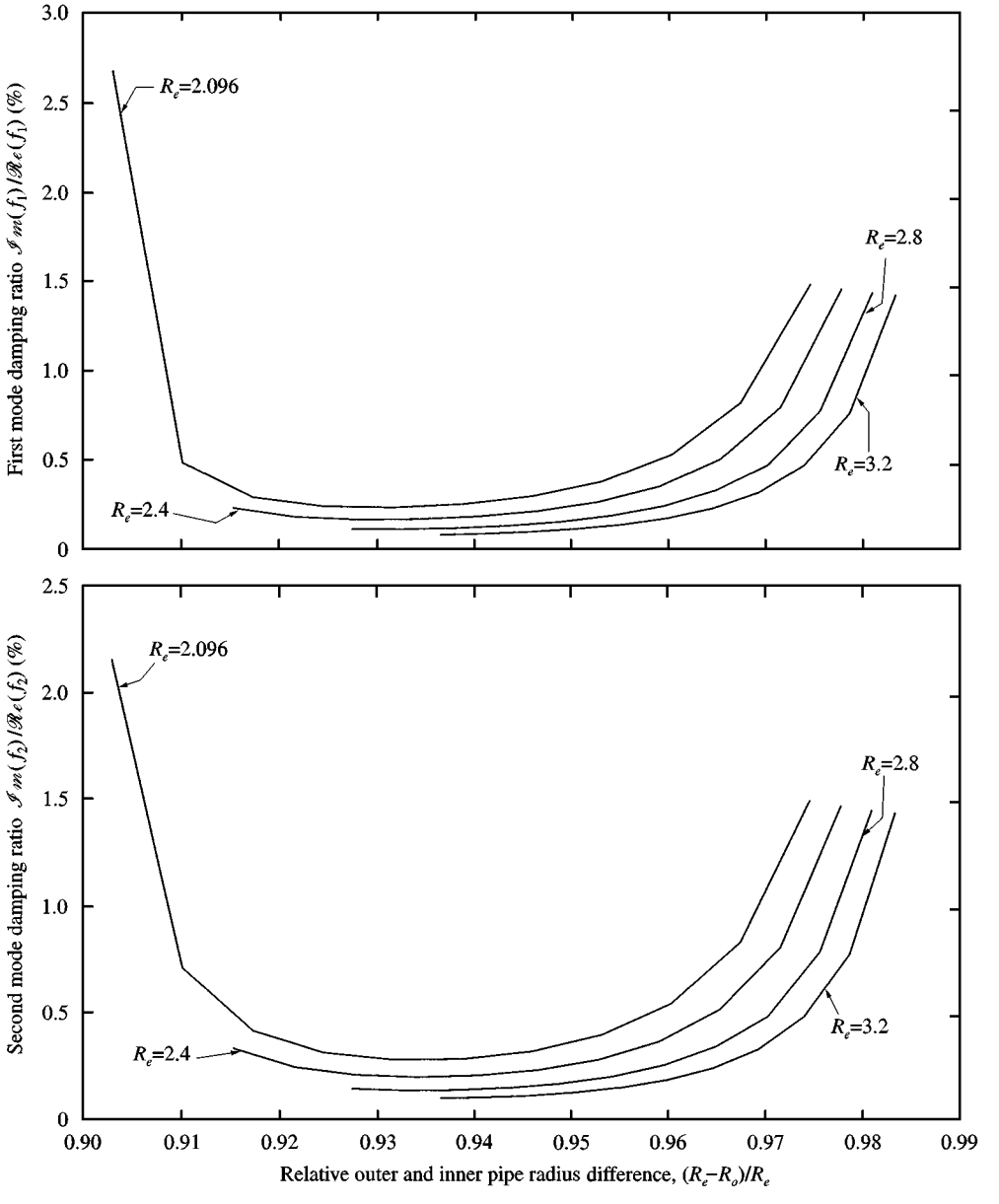

Figure 13. Damping ratio of the first two coupled system frequencies versus relative outer and inner pipe radius difference $(R_e - R_o)/R_e$ (42 grid points).

length. Moreover, calculations show that the inclination angle θ and the depth of the submerged pipe system y_o do not significantly influence the characteristic behavior of the tubular beam.

Concerning the inner pipe radius, Figure 8 shows that for the constant volume flow rates that have been assumed, there exists an optimal radius (around 0·16 m in this case), since we want to maximize the natural frequencies of the inner pipe. Increasing the inner pipe radius increases the pipe stiffness but also increases the external flow velocity and added mass effects. At some point, the velocity and added mass effects overwhelm the stiffening effect, and the inner pipe frequency drops rapidly. In practice, we want to avoid the low frequency and pressure variations introduced by the low-frequency vibration of the inner pipe, which may not be effectively attenuated.

It is also clearly indicated in Figure 9 that as the outer pipe diameter increases, for the constant volume flow rates, the natural frequencies of the inner pipe increase to some plateau. This occurs because reduced confinement lowers the added mass effects on the inner pipe and the external flow velocity decreases until these effects no longer change with increasing outer pipe diameter.

In addition, to further assist in the design of the pipe system, Figures 10, 11, 12 and 13 present the first two frequencies $\mathscr{R}e(f_1)$ and $\mathscr{R}e(f_2)$ and their corresponding damping ratios $\mathscr{I}m(f_1)/\mathscr{R}e(f_1)$ and $\mathscr{I}m(f_2)/\mathscr{R}e(f_2)$ as functions of the relative difference of outer and inner pipe length $(l - L)/l$ and radius $(R_e - R_o)/R_e$ at various outer pipe lengths l and radii R_e, respectively. As shown in Figures 10 and 11, the longer the inner pipe, the lower are the natural frequencies of the inner pipe, but the larger are the damping ratios. The useful design information shown in Figures 12 and 13 worth mentioning is that, with the same outer pipe inner diameter R_e, the smaller the inner pipe diameter represented by R_o, the smaller are the natural frequencies of the inner pipe. However, the change of damping ratio is not monotonic and there exists a region around $(R_e - R_o)/R_e = 0{\cdot}94$ such that the damping ratio is at its lowest level.

5. CONCLUSION

The main contribution of this paper is the formulation of a mathematical model for a submerged concentric pipe system with both unconfined and confined external flows. Using finite-difference schemes, we have calculated the natural frequency range for a given pipe system configuration. It is shown that the proposed method can be used to evaluate the natural frequencies as well as the damping ratios for various design variations. Although, in practice, due to the existence of a pressure pulsation attenuator and other low-pass filters, high-frequency variations can be effectively reduced, we still need to separate other vibration frequencies from the predicted natural frequencies of the inner tubular pipe coupled with the surrounding fluids in order to avoid resonance.

In addition, by varying different design parameters, we conclude that

(i) by decreasing the inner or outer pipe lengths, we can increase the natural frequencies, but changing the inner pipe length is more effective;

(ii) the inclination angle, the depth of the submerged pipe system, and gravity are not important design parameters as far as the pipe dynamical behavior is concerned;

(iii) for a piping system with fixed volume flow rates, there exists an optimal inner pipe radius;

(iv) in general, the larger the outer pipe radius, the more stable the suspended pipe system will be; nevertheless, as the outer pipe radius increases, the inner pipe vibration model approaches that of the case of a singular flexible pipe immersed in an unconfined fluid;

(v) for the same relative outer and inner pipe length difference, the damping ratios increase with the inner pipe length, while for the same relative outer and inner pipe radius difference, the damping ratios decrease with the external pipe inner radius.

The mathematical model presented in this paper clearly shows much promise in achieving a proper design for the silo piping system.

ACKNOWLEDGEMENTS

The authors would like to thank the Institute of Paper Science and Technology and its Member Companies for their support. We are also grateful to Professor D.S. Weaver for his valuable suggestions.

References

Bathe, K. J. 1996 *Finite Element Procedures*. Englewood Cliffs, NJ: Prentice-Hall.

Benjamin, T. B. 1961a Dynamics of a system of articulated pipes conveying fluid. I. Theory. *Proceedings of the Royal Society*, Series A, **261,** 457–486.

Benjamin, T. B. 1961b Dynamics of a system of articulated pipes conveying fluid. II. Experiments. *Proceedings of the Royal Society*, Series A, **261,** 487–499.

Blevins, R. D. 1979 *Formulas for Natural Frequency and Mode Shape*. New York: Van Nostrand Reinhold Company.

Daily, J. W. & Bugliarello, G. 1961 Basic data for dilute fiber suspensions in uniform flow with shear. *TAPPI* **44,** 497–512.

Hannoyer, M. J. & Païdoussis, M. P. 1978 Instabilities of tubular beams simultaneously subjected to internal and external axial flows. *ASME Journal of Mechanical Design* **100,** 328–336.

Hannoyer, M. J. & Païdoussis, M. P. 1979 Dynamics of slender tapered beams with internal or external axial flow. Part I: Theory. *Journal of Applied Mechanics* **46,** 45–51.

Païdoussis, M. P. 1966a Dynamics of flexible slender cylinders in axial flow. Part 1. Theory. *Journal of Fluid Mechanics* **26,** 717–736.

Paidoussis, M. P. 1966b Dynamics of flexible slender cylinders in axial flow. Part 2. Experiments. *Journal of Fluid Mechanics* **26,** 737–751.

Païdoussis, M. P. 1970 Dynamics of tubular cantilevers conveying fluid. *Journal of Mechanical Engineering Science* **12,** 85–103

Païdoussis, M. P. 1973 Dynamics of cylindrical structures subjected to axial flow. *Journal of Sound and Vibration* **29,** 365–385.

Païdoussis, M. P. & Li, G. X. 1993 Pipes conveying fluid: a model dynamical problem. *Journal of Fluids and Structures* **7,** 137–204.

Païdoussis, M. P. & Pettigrew, M. J. 1979 Dynamics of flexible cylinders in axisymetrically confined axial flow. *Journal of Applied Mechanics* **46,** 37–44.

Schlichting, H. 1987 *Boundary-Layer Theory*, 7th edition. New York: McGraw-Hill.

Taylor, G. 1952 Analysis of the swimming of long and narrow animals. *Proceedings of the Royal Society*, Series A, **214,** 158–183.

Wang, X. & Bloom, F. 1999. Stability issues of concentric pipes conveying steady and pulsatile fluids. *Journal of Fluids and Structures* (under review).

Wang, X., Feng, Z. & Forney, L. J. 1999 Computational simulation of turbulent mixing with mass transfer. *Computers & Structures* **70,** 447–465.

Zienkiewicz, O. C. 1977 *The Finite Element Method*, 3rd edition. New York: McGraw-Hill.